Chemical Geology 648 (2024) 121954

Contents lists available at ScienceDirect

Chemical Geology

journal homepage: www.elsevier.com/locate/chemgeo

Roles of changes in land weathering intensity in the Nd cycle of the South China Sea during the past 30 kyr as inferred from neodymium isotopic composition in foraminifera

Yi Huang [a], Christophe Colin [a,*], Zhifei Liu [b], Bertaz Joffrey [a,b], Arnaud Dapoigny [c], Eric Douville [c], Zhaojie Yu [d], Andrew Tien-Shun Lin [e]

[a] *Université Paris-Saclay, CNRS, GEOPS, 91405 Orsay, France*
[b] *State Key Laboratory of Marine Geology, Tongji University, Shanghai 200092, China*
[c] *Laboratoire des Sciences du Climat et de l'Environnement, LSCE/IPSL, CEA CNRS-UVSQ, Université Paris-Saclay, F-91191 Gif-sur-Yvette, France*
[d] *Key Laboratory of Marine Geology and Environment, Institute of Oceanology, Chinese Academy of Sciences, Qingdao 266071, China*
[e] *Department of Earth Sciences, National Central University, Jhongli, 32001, Taiwan.*

ARTICLE INFO

Editor: Christian France-Lanord

Keywords:
Foraminiferal εNd
Weathering
River discharge
Paleohydrology
East Asian Summer Monsoon
South China Sea

ABSTRACT

Neodymium isotopic compositions (εNd) in the marginal sea is influenced by the ocean circulations as well as the lithogenic input from continents, but their relative contributions and the impact of detrital sediments are not well constrained. In this study, Nd isotopic compositions of mixed planktonic foraminifera species and carbonate-free fraction of sediment from two cores collected at 1250–1350 m water depth in the southwestern (core MD01–2393) and northeastern (core MD18–3569) South China Sea (SCS) have been investigated in order to constrain the relative contributions of lithogenic Nd inputs from large Asian rivers and hydrological variations at intermediate depth in the SCS. The foraminiferal εNd values of both cores (-7.3 ± 0.2 to -5.8 ± 0.2 for core MD18–3569 and -8.1 ± 0.2 to -7.2 ± 0.2 for core MD01–2393) indicate strong modifications of the initial εNd of the North Pacific Intermediate Water (NPIW) (εNd of −4) flowing into the SCS by unradiogenic sediments (−13 to −11) from large Asian rivers. The foraminiferal εNd record of core MD01–2393 displays significantly unradiogenic values from 18 to 8 cal kyr BP which are associated with intensification of monsoon rainfall and river input of detrital material characterized by strongly altered minerals (high illite chemical index and kaolinite/illite ratio) deriving from tropical plain soils of the Mekong River basin. We suggest here that pedogenetic minerals from tropical plain soils are more efficient in terms of Nd exchange with the seawater than primary minerals produced by intense physical erosion during the glacial period. In contrast, the foraminiferal εNd record for the northern core MD18–3569 is characterized by radiogenic εNd values from 18 to 12 cal kyr BP; these values have been linked to an increased intrusion of radiogenic glacial NPIW to the northern SCS and greater ventilation of water masses (deduced from $\Delta^{14}C$) in the northern deep basin of the SCS compared to the southern one. This time interval is associated with newly formed NPIW in the subarctic Pacific Ocean beginning at about 18 cal kyr BP. Overall, our results indicate that the state of chemical weathering of sediment delivered by rivers is the main factor controlling the detrital modification of past seawater εNd distributions in the marginal sea of the SCS.

1. Introduction

The South China Sea (SCS) is a key area for reconstructing high-resolution paleo-hydrological and paleoclimatic variability in the tropical western Pacific at different time scales. It is significantly influenced by the water current from the western Pacific (Wyrtki, 1961; Qu et al., 2006), as well as large inputs of weathered materials from south China margins which are formed by the uplift of the Tibetan Plateau (Milliman and Farnsworth, 2011; Liu et al., 2016).

The SCS is a semi-closed marginal sea connected to the western Pacific Ocean through a single channel, the Luzon Strait, which is the only passage for the North Pacific Intermediate and deep-water masses

* Corresponding author.
E-mail address: christophe.colin@universite-paris-saclay.fr (C. Colin).

https://doi.org/10.1016/j.chemgeo.2024.121954
Received 11 April 2023; Received in revised form 15 January 2024; Accepted 19 January 2024
Available online 20 January 2024

(NPIW and PDW) to enter (Wyrtki, 1961; Qu et al., 2006). These intermediate and deep-water masses first turn northwestward before flowing southward along the continental margin off Southeast China (Qu et al., 2006) and contribute to the SCS Contour Current (Zhao et al., 2015). Several previous studies have investigated high resolution sequences in the northern and western margin of the SCS to study the paleohydrology of water masses inflowing into the SCS at different time scales (Jian et al., 1999; Li et al., 2004; Yin et al., 2021; Zheng et al., 2016), mainly using typical proxies (e.g. $\delta^{13}C$ or $\Delta^{14}C$ analyzed on foraminifers, sortable silts…) (e.g. Wan et al., 2018; Wan and Jian, 2014; Wan et al., 2020; Zhao et al., 2023). These studies indicate that the glacial NPIW became the most prominent source of deep water in the SCS after the last glacial maximum (LGM, 18–24 kyr) (Wan et al., 2018; Wan and Jian, 2014), which is associated with strengthened mid-depth circulation in the North Pacific resulting from the formation of the glacial NPIW in the subarctic Pacific (Matsumoto et al., 2002; Okazaki et al., 2012).

In the last two decades, Nd isotopic composition ($^{143}Nd/^{144}Nd$ expressed as εNd) has been shown to be a useful proxy to track water mass circulation of the ocean due to the "quasi conservative" behaviour of Nd in seawater (Frank, 2002; Piotrowski et al., 2005; Tachikawa et al., 2014; Dubois-Dauphin et al., 2017; Fuhr et al., 2021; Montagna et al., 2022). Several studies have thus tentatively investigated εNd analyzed on authigenic and biogenic phases of sediments from the deep depth (>1500 m) of the SCS in order to better constrain the origin of water masses at different time scales (Huang et al., 2014; Wu et al., 2015b; Wu et al., 2017). It has been demonstrated that the deep-water in the SCS mainly consists of the inflow through the Luzon Strait of the PDW and NPIW, which today are characterized by similar Nd isotopic compositions to those of the Western Pacific Ocean (e.g. Philippine Sea) (around −4; Wu et al., 2015a, 2022). Any variations in the paleohydrology of the Pacific Ocean, which are characterized by contrasted Nd isotopic composition between southern sources water masses (e.g. AAIW = −8 to −6; UCDW/LCDW = −9 to −7, Jeandel et al., 2013, Carter et al., 2012) and northern sources water masses (NPIW = −3.4 ~ − 2.7 and NPDW = −4, (Amakawa et al., 2004, 2009) should be recorded in the SCS, at least in its northern part. Unfortunately, the record of past intermediate water in the SCS is poorly constrained.

However, close to the continent, seawater Nd isotopes are strongly influenced by continental weathering, whose signature is directly imprinted on local intermediate and deep water via dissolved riverine inputs, scavenging and desorption of sinking particles in the water column (Grasse et al., 2012; Stichel et al., 2015; Wang et al., 2021), as well as benthic fluxes in ocean margin sediments (Abbott et al., 2016; Du et al., 2016). Therefore, seawater εNd in marginal seas may reflect the combined effect of regional lithogenic inputs from continental weathering and mixing of water masses characterized by distinct isotopic signatures (Jeandel et al., 2007; Montagna et al., 2022; Rousseau et al., 2015; Osborne et al., 2014). Recent studies have shown that dissolved seawater εNd distribution in the Bay of Bengal displays a north-south gradient with a seasonal variability resulting from monsoonal variability of the input of unradiogenic lithogenic Nd from large Himalayan rivers (mainly the Ganges–Brahmaputra river system) and the inflowing water masses originating from the Southern Ocean (Singh et al., 2012; Yu et al., 2017b). This particularly enables us to constrain the relative contributions of lithogenic Nd inputs from the Himalayas during the Quaternary (Burton and Vance, 2000; Gourlan et al., 2008, 2010; Bang et al., 2021; Yu et al., 2017b, 2022). Nevertheless, some important issues regarding the specific mechanism of how these two factors co-affect the seawater εNd remain unresolved.

In addition, several previous studies infer that the interaction between dissolved and particulate phases could be dependent on the mineralogy of the lithogenic input to the ocean and/or the state of chemical weathering of the lithogenic material (Blanckenburg and Nagler, 2001; Howe et al., 2016; Hindshaw et al., 2018; Larkin et al., 2021; Wang et al., 2022; Bayon et al., 2023; Huang et al., 2023). For example, the labile Nd bearing materials derive mainly from sedimentary sources rather than the dissolution of silicate minerals (Jang et al., 2020), thus the erosion and weathering of sedimentary rocks might promote the reactivity of the labile fraction and its exchange with dissolved seawater (Larkin et al., 2021). Nevertheless, some important issues regarding the mineralogy fractions that are able to exchange Nd with seawater are still unsolved.

The SCS receives a huge amount of suspended sediments (~700 million tons annually) from surrounding drainage basins, representing 3.7% of estimated global fluvial sediment discharge into the world ocean (Milliman and Farnsworth, 2011). These huge river basins deliver to the SCS sediments that are characterized by very contrasted mineralogical (clay mineral assemblages) and geochemical compositions (Liu et al., 2016). Quaternary sediments of the SCS have been intensively investigated using sediments sampled off-shore from large Asian rivers (e.g. Mekong River, Pearl River etc.) in order to establish past changes in weathering and sediment transfer to the oceanic margin (Liu et al., 2010, 2016; Colin et al., 2010; Hu et al., 2012; Chen et al., 2017; Zhao et al., 2018). These studies reveal a close relationship between the weathering/erosion process and climate changes (e.g. East Asian Monsoon and sea-level variations) (Boulay et al., 2005; Chen et al., 2017; Zhao et al., 2018; Jiwarungrueangkul and Liu, 2021). As a result, the SCS constitutes an ideal area to better constrain the specific processes and sources involved in the exchange between seawater and river detrital sediments, aspects that currently remain unclear.

Given that the deep water masses flow along the continental margin off southeast China after entering the SCS from the Luzon Strait (Qu et al., 2006) and since there are large detrital discharges from the Pearl River, Red River, and Mekong River characterized by negative εNd values (−13 ~ −10.7, Wei et al., 2012) compared to the NPIW or PDW (around −4 ~ −3, Amakawa et al., 2004), it follows that the εNd of SCS intermediate and deep-waters could be strongly modified by unradiogenic lithogenic Nd inputs during its southward circulation in the SCS. Such Nd isotopic composition modification is particularly well observed in modern surface seawater which yields less radiogenic εNd values in the southern SCS (−9.5 ~ −7.1) compared to the northern basin (−5.3 ~ −3.3; Amakawa et al., 2000, Wu et al., 2015a). Such north-south gradient of seawater εNd has been also observed indirectly for deep water of the SCS through foraminiferal εNd values extracted from core top sediments in northern (MD05–2904, 2066 m, εNd = −4.2 ± 0.3) and southern SCS (MD05–2899, 2393 m, εNd = −6.2 ± 0.4; MD05–2901, 1454 m, −7.2 ± 0.2, Wu et al., 2015b). During glacial-interglacial cycles of the Quaternary, changes in the paleogeography of the SCS due to lowered sea-level, variations in weathering state of sediments, variations in sediment flux to continental margins and changes in water exchanges between the Philippines Sea and the SCS, as well as hydrological changes within the SCS, could have modified the spatial distribution of seawater εNd in the SCS. However, the lack of εNd records at intermediate depth for the area close to the Luzon Strait and for the southern SCS does not permit to distinguish, in past seawater εNd record of the SCS, the contribution of variations induced by water masses mixing from lithogenic Nd input resulting from continental weathering.

In this study, εNd values of mixed planktonic foraminifera have been analyzed on two sediment cores located in the northeastern and southwestern SCS to establish the relative contributions of lithogenic Nd input from rivers (southern Taiwanese rivers and the Mekong River) and contributions from the intermediate-water inflows from the north Pacific during the last 25 kyr. In a broader context, the εNd records are compared with previous Sea Surface Salinity records and mineralogical proxy records of the intensity of chemical weathering affecting river basins (Liu et al., 2005; Colin et al., 2010; Chen et al., 2021) in order to determine, in an exploratory way, the potential relationship between foraminiferal Nd isotope compositions and the state of chemical weathering of detrital materials transported to the SCS and their link with past climate changes (e.g., East Asian Monsoon and sea-level variations).

2. Hydrological setting and materials

2.1. Hydrological setting

The SCS is a completely isolated basin below the deepest 2400 m sill in the Luzon Strait (Qu et al., 2006; Wyrtki, 1961). The deep SCS water derives from the intrusion of the PDW with high salinity (34.62) and a low temperature (1.68 °C). The PDW (2000–2500 m) sinks immediately after crossing the Luzon Strait and joins a basin-scale cyclonic deep circulation (Qu et al., 2006; Tian et al., 2009; Wang et al., 2011). The NPIW, characterized by higher temperatures and lower salinity (34.15), overlies the PDW (Tian et al., 2009). The present-day mean trajectory of intermediate water in the Luzon Strait is eastward with strong seasonal variability (Xie et al., 2011; Zhu et al., 2019). According to the basin-scale oxygen distribution and numerical model simulations, the deep water flows northwestward to the northern slope of the SCS and thereafter southwestward along the western margin of the SCS (Fig. 1a,b) (Li and Qu, 2006; Qu et al., 2006; Wang et al., 2018). This southwestward movement of intrusive water ends at approximately 13°N, along the slope east of Vietnam where the intermediate water extensively subducts downward (Liu and Gan, 2017). The intermediate and deep-water masses of the SCS present a general anticlockwise circulation along all margins of the SCS inducing a mixing of water masses from the northern and southern SCS (Fig. 1b). Enhanced vertical mixing and the cyclonic circulations suggest a much shorter residence time of deep water in the SCS (30–50 yrs., Chang et al., 2010) than that of the Pacific Ocean (~1000 yrs., Broecker et al., 2008). A recent estimation indicates that deep water in the southern SCS has a longer residence time (~40 yrs) than that of the northern SCS (~25 yrs., Liu and Gan, 2017). Strong vertical deep mixing between intermediate and deep water and lateral advection occurred in the southern SCS during the Holocene (Wan and Jian, 2014; Jin et al., 2018).

The climate of the SCS and its surrounding continents is primarily affected by the East Asian Monsoon. The East Asian Monsoon results from differential land-sea heating and induces seasonal reversal in wind direction and sea surface circulations of the SCS, as well as a seasonal variation in precipitation, runoff, and freshwater and sediment discharges to the SCS (Wang et al., 2005). The SCS (including Taiwanese rivers and the Mekong River basin) is thus characterized by a humid summer monsoon period from about May to October and a drier winter monsoon period from November to April (Wang et al., 2001; Wang et al., 2005).

The SCS receives a huge amount of suspended sediments (>700 Mt./yr) from large Asian River basins (e.g. Mekong River, Red River, Pearl River etc), triggering high sediment accumulation rates throughout the SCS (Liu and Stattegger, 2014). Sediment discharge rates from Taiwanese rivers and the Mekong River to the SCS are 176 Mt./yr and 160 Mt./yr, respectively (Liu et al., 2016). On the one hand, rivers in southern Taiwan are generally short in length and are characterized by small drainage basins, steep slope gradients and highly erodible bedrock (Wang et al., 2009). Taiwan is characterized by strong physical erosion and sediments delivered to the SCS are characterized by poorly hydrolyzed minerals. Sediments discharged from southern Taiwan are then transferred to the deep basin by turbidity currents along deep-sea canyons, e.g., the Gaoping Canyon. At the present time, turbidity currents in the Gaoping Canyon are largely controlled by typhoon events (Zhang et al., 2018). On the other hand, the Mekong River originates from the Tibetan Plateau and flows southeastwards through steep valleys along the eastern Tibetan margin into the vast plains of Indochina before entering the SCS (Liu et al., 2007). The upper catchment of the Mekong River is associated with strong physical erosion, delivering mainly poorly hydrolyzed minerals, whereas soils of the lower reaches of the Mekong River basin supply contrasted mineralogy associated with tropical soils. Accumulated discharges during the wet season (~4 months from June to September) from the Gaoping River and Mekong River account for approximately 78% and 85% of the total annual discharge, respectively. This corresponds to suspended loads that are ten times higher in wet seasons than in dry seasons (Wang et al., 2009; Duy Vinh et al., 2016). Due to a large influx of freshwater during the wet summer monsoon, a sea surface salinity reduction (up to ~7‰) can be observed in the SCS, particularly along a latitude of 17°N (Levitus et al., 1994).

2.2. Sediment cores and age models

The Calypso cores MD18–3569 (22°09.30′N; 119°49.24′E; water depth of 1320 m; 40.08 m long) and MD01–2393 (10°30.15"N; 110°03.68″E; water depth of 1230 m; 42.5 m long) were collected off southwest Taiwan during the HydroSed cruise in July 2018 and in the southwestern SCS during the 122/IMAGES VII-WEPAMA cruise in 2001 aboard the R/V *Marion Dufresne*, respectively (Fig. 1b). These study sites have been selected because they each receive detrital sediments from a single main sedimentary source. Core MD18–3569 is located on the southeastern bank of a meander of the Penghu Canyon at ~600 m of altitude above the canyon thalweg which means that overspilling turbidity currents do not reach the site. The lithology of the core consists of a homogenous hemipelagic brown clay without any visible turbidites. Core MD01–2393 is located on the continental slope, ~400 km off the modern Mekong River mouth. The lithology is homogeneous and ranges from olive/dark clay to silt with foraminifer-rich or diatom-bearing nannofossil ooze. Both cores are located above the depth of the Luzon Strait (2400 m) and in a similar intermediate water masse corresponding to the NPIW that flows along the northern and western margins of the SCS.

The age models of cores MD18–3569 and MD01–2393 were based both on the $\delta^{18}O$ stratigraphy of the planktonic foraminifera *Globigerinoides ruber* and on accelerator mass spectrometry (AMS) ^{14}C dates obtained on well-preserved calcareous tests of planktonic foraminifera *Globigerinoides ruber* or *Globigerinoides sacculifer* (Fig. 2a,c) (Colin et al., 2010; Chen et al., 2021).

The mean sedimentation rate of core MD18–3569 is high (54.7 cm/kyr) and increases significantly during the last deglaciation from 34.9 to 52 cm/kyr, reaching a maximum value of 72.9 cm/kyr after 4 cal kyr BP (Fig. 2b) (Chen et al., 2021). Core MD01–2393 provides a continuous record since the last 25 cal kyr BP with an average sedimentation rate of about 40 cm/kyr (Fig. 2d) (Colin et al., 2010). Both studied cores are characterized by high sedimentation rates allowing us to obtain a high temporal resolution for εNd analyses spanning the last 25 cal kyr BP.

3. Methods

Approximately 30 mg of mixed planktonic foraminifera from sediment samples of cores MD01–2393 and MD18–3569 were picked from the >150 μm fraction for Nd isotope analyses. The samples were gently crushed between two glass slides under the microscope to open all chambers, and then ultrasonicated with Milli-Q water. Each sample was rinsed thoroughly with Milli-Q water to remove the supernatant and the procedure was repeated until the solution was clear and all clay had been removed. After the cleaning step, samples were dissolved using stepwise 100 μl diluted nitric acid (1 N) until the dissolution reaction completed. The dissolved foraminifera were centrifuged, and the supernatant was immediately transferred to Teflon beakers to prevent leaching of any possible remaining phases.

In addition, Nd isotopic compositions were analyzed on 9 sediment samples from core MD18–3569 after decarbonation (20% acetic acid) and organic matter removal (H_2O_2). Samples were firstly dissolved in HF-$HClO_4$ and HNO_3-HCl mixtures.

Nd was then separated following the analytical procedure described in Copard et al. (2010). Samples were first loaded on preconditioned TRU Spec columns to elute unwanted cations using five aliquots of 0.5

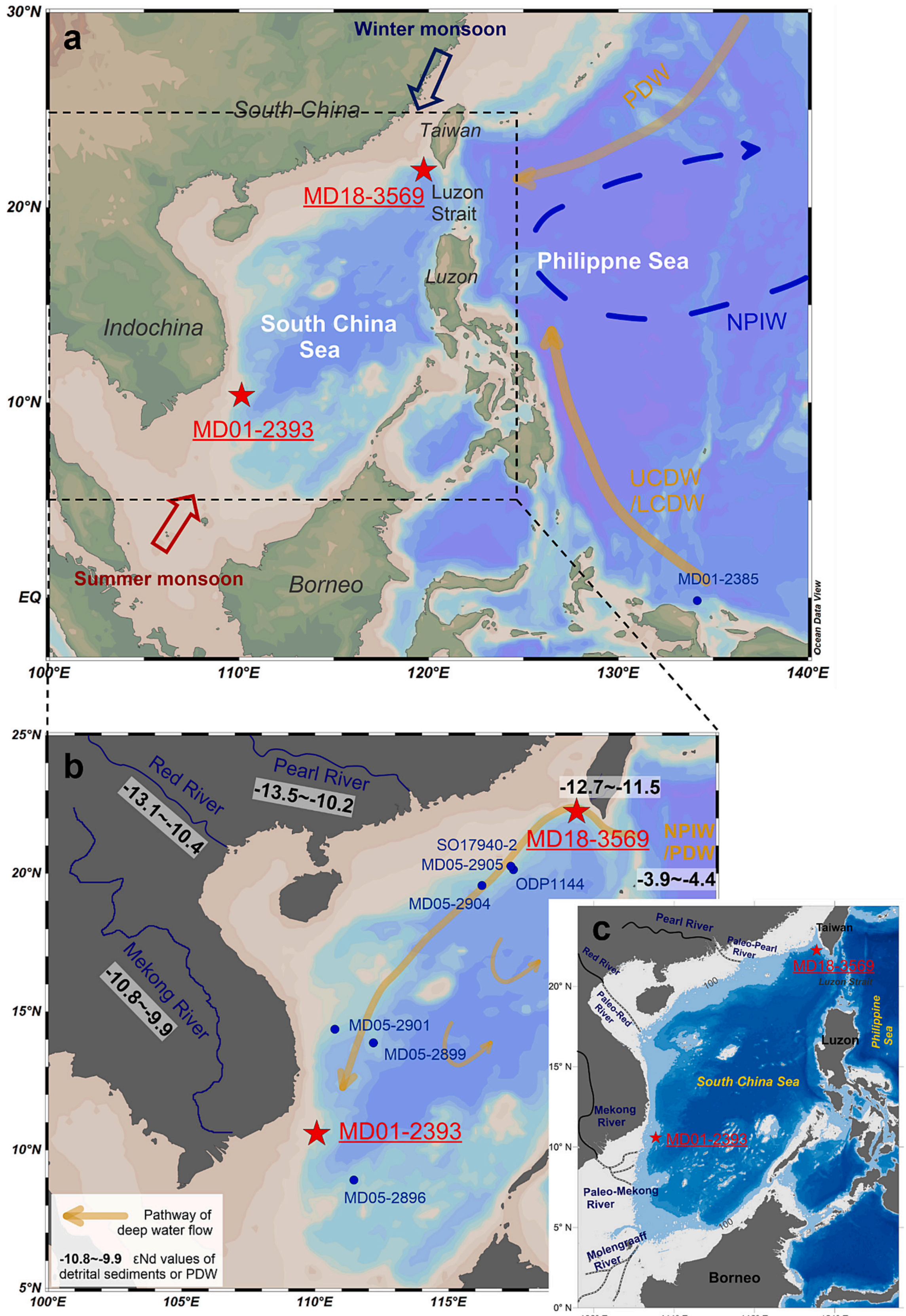

Fig. 1. Geographical setting and locations of cores MD01–2393 and MD18–3569 (red Pentagrams). The gold line and the blue dashed line in panel (a) indicate the circulation of deep water and intermediate water in the Pacific Ocean which flow into the SCS through the Luzon Strait (Kawabe and Fujio, 2010). The gold line in panel (b) indicates the dominant anticlockwise circulation of deep current in SCS. The locations of other cores discussed this study are shown by blue circles (Boulay et al., 2005; Wu et al., 2015a, 2015b, 2017; Huang et al., 2014; Zhao et al., 2023). (c) Paleogeography of the SCS during the Last Glacial Maximum (LGM). Paleo-river systems are reported (Wang et al., 2005). (For interpretation of the references to colour in this figure legend, the reader is referred to the web version of this article.)

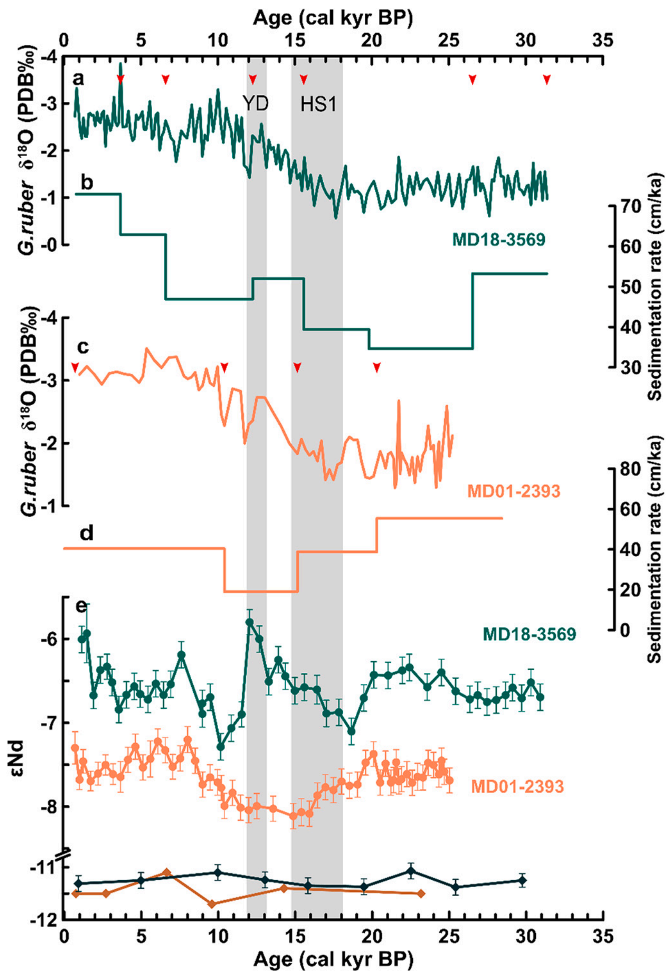

Fig. 2. Age- *G. ruber* $\delta^{18}O$ plots for core MD18–3569 (a) and core MD01–2393 (c) respectively. The red triangles represent AMS 14C age dating points (Liu et al., 2005; Chen et al., 2021); The sedimentation rate for core MD18–3569 (b) and core MD01–2393(d); (e) εNd of mixed planktonic foraminifera obtained from cores MD18–3569 and MD01–2393; εNd of organic material and carbonate-free fraction of sediment from cores MD18–3569 (this study) and MD01–2393 (Liu et al., 2005). The terms YD (~12.8 to 11.7 kyr BP) and HS1 (~18 to 14.7 kyr BP) corresponds to periods of the Younger Dryas and Heinrich Stadial 1 events, respectively. (For interpretation of the references to colour in this figure legend, the reader is referred to the web version of this article.)

ml 1 M HNO_3; the TRU spec columns were then placed over Ln-Spec columns. The LREEs were eluted from the upper (TRU spec) columns using seven aliquots of 0.1 ml 0.05 M HNO3. After decoupling from the Ln Spec columns, 2.5 ml of 0.25 M HCl was used to elute La, Ce and most of the Pr. Nd were then eluted with an additional 3.25 ml 0.25 M HCl.

The $^{143}Nd/^{144}Nd$ ratios of all purified Nd fractions were measured using the Multi-Collector Inductively Coupled Plasma Mass Spectrometer (MC-ICP-MS Neptune^{Plus} Thermo Fisher) (PANOPLY's analytical facilities at the University Paris-Saclay, France) hosted at the *Laboratoire des Sciences du Climat et de l'Environnement* (LSCE, Gif-sur-Yvette, France). The solutions were analyzed at a concentration of 10 to 15 ppb. The mass-fractionation correction was made by normalizing $^{146}Nd/^{144}Nd$ to 0.7219 and applying an exponential-fractionation law correction. During the analysis, every group of three samples was bracketed with JNdi-1 with Nd concentrations similar to those of samples. Replicate analyses of the JNdi-1 standard yielded mean $^{143}Nd/^{144}Nd$ ratios of 0.512105 ± 0.000007 (2σ, $n = 35$), matching the well accepted values of 0.512115 ± 0.000006 (Tanaka et al., 2000) for JNdi-1. The εNd external reproducibility (2σ) deduced from repeated measurements of the JNdi-1standard, is below 0.2 epsilon units for the different analytical sessions. The analytical uncertainty is the combination of the reproducibility of the session standard and the measurement error of each sample. Total blank values were < 30 pg and can be ignored as they represent <0.1% of the sample characterized by the lowest quantity of Nd.

4. Results

For core MD18–3569, located in the northeastern SCS, εNd values of bulk siliciclastic sediments display a narrow range from −11.1 ± 0.2 to −10.4± 0.2 (Table S1 and Fig. 2e). In contrast, foraminiferal εNd display a large range from −7.3 ± 0.2 to −5.8 ± 0.2 over the last 31 kyr (Fig. 2e). In general, samples from the last glacial period have similar εNd values to those of the mid-Holocene. The time interval from 20 to 18.6 cal kyr BP is associated with a negative shift of εNd values reaching up to −7.1 ± 0.2. This is followed by a subsequent progressive increase from 18 to 12 cal kyr BP to reach a maximum (−5.8 ± 0.2) during the time interval coeval with the Younger Dryas event in Europe. Thereafter, a second negative excursion of around 1.5 units to a minimum εNd value (−7.3 ± 0.2) is observed between 12 and 10.2 cal kyr BP. The early Holocene (from 10.2 to 7.6 cal kyr BP) is characterized by a gradual increasing trend towards higher εNd values. During the mid to late Holocene, εNd values display a narrow range (from −6.9 ± 0.2 to −5.9 ± 0.3) with slight variations.

For core MD01–2393, located in the southwestern SCS, foraminiferal εNd values range from −8.1 ± 0.2 to −7.2 ± 0.2 over the last 25 kyr, values that are significantly less radiogenic than those of core MD18–3569 (mean value of −7.7 ± 0.2, $n = 56$ for core MD01–2393 vs mean value of −6.6 ± 0.2, $n = 49$ for core MD18–3569) (Fig. 2e). In general, the Nd isotopes are slightly less radiogenic during the deglacial period (between −8.1 ± 0.2 and − 8.0 ± 0.2) than during the last glacial (between −7.5 ± 0.2 and − 7.7 ± 0.2) and Holocene (between −7.2 ± 0.2 and − 7.7 ± 0.2) periods.

5. Discussion

5.1. *εNd values of foraminifera in the SCS: local detrital signal*

εNd values of planktonic foraminifera are shown to record the Nd isotope composition of bottom and/or porewater rather than the ambient seawater at calcification depth (Pomie's et al., 2002; Tachikawa et al., 2014; Yu et al., 2018; Abbott et al., 2019). This is due to the presence of authigenic Fe—Mn oxides and hydroxides precipitated onto the carbonate shells (Roberts et al., 2010; Piotrowski et al., 2012). These coatings cannot be easily eliminated by oxidative/reductive cleaning procedures (Roberts et al., 2012; Kraft et al., 2013; Wu et al., 2015b). Therefore, εNd values measured on mixed planktonic foraminifera can be used as a tracer for reconstructing past deep-water circulations even if the possibility of pore water Nd influence should be keep in mind for some regions (Tachikawa et al., 2014). Previous core-top εNd records of planktonic foraminifera collected in the northern SCS are identical to modern seawater εNd values at deep depth (e.g. for core MD05–2904) (Wu et al., 2017), which suggests that εNd values obtained on fossil planktonic foraminifera record the deep-water Nd isotope signature of the PDW flowing into the SCS.

εNd values for uncleaned planktonic foraminifera collected from cores over an extensive area in the north-western Pacific suggest that there is no major change in Holocene and LGM εNd values (Hu et al., 2016), which indicates that εNd values of NPDW show no significant difference between the last glacial and the Holocene (between −1.6 ± 0.1 and − 3.1 ± 0.1). Core MD01–2385 (0.22°S, 134.24°E, 2602 m water depth), located on the pathway of UCDW (Upper Circumpolar Deep Water) entering the southern Philippine Sea, is characterized by radiogenic εNd values of between −2.9 and − 1.9 which remained relatively constant over the last 30 kyr (Wu et al., 2017). In addition, given that the Luzon Strait is very wide and characterized by a depth of around 2400 m, glacial-interglacial changes of the sea level (∼120 m) cannot significantly modify water masses exchange and then Nd flux between the Philippine Sea and the SCS. This implies that the εNd records in the northern SCS cannot be explained by a temporal change in the Nd isotopes and/or the Nd flux of the deep-water which has been flowing into the SCS since the last glacial period.

The foraminiferal εNd values of the core-tops from MD18–3569 (1320 m) and MD01–2393 (1230 m) are −6.0 ± 0.2 and − 7.3 ± 0.2 respectively. Such values are 2–3 εNd units less radiogenic than modern NPIW or PDW flowing through the Luzon Strait (−3.4 ∼ −4.2; Wu et al., 2022). Similar negative εNd values have been observed previously on foraminifera from core top MD05–2901 (εNd = −7.2 ± 0.2; 14.28°N, 110.74°E, 1454 m water depth) and MD05–2899 (εNd = −6.2 ± 0.4; 13.79°N, 112.19°E, 2393 m water depth), which are located in between the two sites studied here (Wu et al., 2015b). Core MD18–3569 is located close to Taiwan canyon characterized by frequent turbidity currents such as for the Gaoping canyon (Zhang et al., 2018). The southern margin of Taiwan is also associated with strong deep-sea currents and the presence of abundant benthic and intermediate nepheloid layers (Huang et al., 2023). This core is then presumed to receive more lithogenic discharge from Taiwanese rivers than core MD05–2904 in the northern SCS. Consequently, the core-top foraminiferal εNd could be greatly modified by unradiogenic terrigenous fractions. εNd values of the deep-water mass are considerably modified during its pathway along the margin of southern China by seawater exchange with unradiogenic sediments (−9 ∼ −13.5, Wei et al., 2012, Liu et al., 2016) delivered by large rivers (e.g., Pearl River, Red River and Mekong River). This results in core-top εNd values in core MD01–2393 in the southern SCS that are less radiogenic than those in core MD18–3569 in the northern SCS (Fig. 2). This confirms that sediments discharge from continents plays an important role in past dissolved εNd values of bottom waters in the SCS (Wu et al., 2017). However, unfortunately, dissolved εNd of seawater just above the sediment interface of both studied sites and more generally in the southern SCS are not yet available. We cannot distinguish whether the foraminiferal εNd imprint only the Nd isotopic signature of the seawater and/or significant affected by benthic fluxes. Consequently, benthic flux as well as seawater exchange with particles in the water column could be responsible to the negative offset observed between foraminiferal εNd and the Nd isotopic composition of the PDW with entrance in the SCS through the Luzon Strait. On the basis of Sr and Nd isotopic compositions obtained from the detrital fraction, it has been shown that, over the last 25 cal kyr BP, the main sedimentary source of core MD01–2393 has been the Mekong River (Liu et al., 2005). In addition, the input of Mekong River sediment to the southern SCS has recently been confirmed from clay mineralogy and Sr - Nd isotopic compositions obtained from core MD05–2896 collected at greater water depth in the deep-basin of the southern SCS (Fig. 1b) (Sang et al., 2022). Core MD18–3569 mainly derived from southern Taiwanese rivers and may have been transferred to the studied site through deep-sea canyons such as the Gaoping Canyon. The εNd values of the detrital fraction of both cores exhibit a narrow range from −11.1 to −11.7 for core MD 01–2393 and − 11.1 to −10.4 for core MD18–3569, respectively (Fig. 2e). They are similar to εNd of the sediments at river mouth (∼ − 11.2 for Mekong River, Liu et al., 2005; −12.7 ∼ −11.5 for Taiwanese rivers, Wei et al., 2012). Consequently, detrital sediments deposited in each of the studied cores have derived from a unique and constant sedimentary source over the last 30 kyr.

The large variations of up to 1.5 εNd units in the seawater εNd records cannot be linked to any changes in the εNd of the detrital fraction which has remained quasi constant during the last 25 cal kyr BP for both studied cores. In addition, we can hypothesize that if there is a benthic flux influence, it should be characterized by a Nd isotopic composition close to that of the detrital fraction of both cores. It also seems reasonable to exclude a major impact of diagenesis processes on foraminiferal εNd variations of the two studied sites. We are aware that detrital fraction is heterogeneous and it is possible that εNd values of residual detrital fraction do not represent the values of labile detrital phases that may affect pore Nd isotopic signature (Blaser et al., 2016). Considering this difficulty, we argue our two hypotheses based on the following reasons. Cores MD12–2393 and MD18–3569 show similar trends of εNd variations at 20–18 cal ka BP with a decrease of the εNd and at 10–8 cal ka BP with an increase of the εNd. εNd records display several millennial variations at the same time for cores MD12–2393 and MD18–3569 after 7 cal ka BP (Fig. 2). In the northern SCS, foraminiferal εNd of core MD18–3569 presents similar pattern of variations with cores MD05–2904 and SO17940–2 suggesting a regional signal of the εNd variations and not a local one. All these cores derive from different river systems (Pearl River, Mekong River and Gaoping River), are characterized by different sedimentation rates and different marine environments. The diagenesis of the sediments in all these cores cannot therefore be associated with a similar diagenesis process that evolves over time with the same chronology. We can conclude that changes in the seawater εNd record cannot be attributed only to a modification of the sedimentary source or of effect of diagenesis and should be attributed to changes in the flux of sediments and/or in the mineralogy of sediment transported to the deep-sea margin since the last glacial period.

5.2. Constraints on the variations in foraminiferal εNd values in the southern SCS

For core MD01–2393, the deglacial period (18–12 cal kyr BP) is associated with the most negative εNd values, while the last glacial period and the Holocene are characterized by similar and higher radiogenic εNd values (Fig. 3b). Such variations for foraminiferal εNd values suggest an intensive modification of detrital sediment inputs from the Paleo-Mekong River and the Molengraaff River during the deglacial period (Fig. 1c). This modification can be related to the variations in sediment flux and the efficiency of exchange between detrital sediments and seawater.

5.2.1. Flux of sediment discharges

It has been shown that dissolved εNd of marginal seas of large river systems, such as the Ganges-Brahmaputra Rivers, could be modified by lithogenic Nd inputs from both freshwater and sediment discharges from rivers >1000 km away from the river mouth and to a depth of >2000 m (Yu et al., 2017a; Yu et al., 2017b). Seasonal changes in the seawater εNd of the Bay of Bengal have also been observed and have been linked to Indian monsoon and subsequent seasonal variations in the Ganges-Brahmaputra River inputs (Yu et al., 2017b). Such previous studies highlight a very rapid exchange of Nd between riverine particles and seawater and indicate that it is possible for the ocean to be modified at the scale of a season through a modification of terrigenous river fluxes. Taking into account the huge sediment discharge of the Asian rivers to the southern SCS, we can reasonably suggest that lithogenic Nd inputs from these major Asian river systems must have modified the glacial seawater εNd of the southern SCS.

The $\delta^{18}O$ of the surface seawater ($\delta^{18}O_{sw}$) established from core MD01–2393 after corrections of local sea surface temperature based on alkenone thermometer and global ice-sheet volume variations record the local freshwater budget from the Mekong River (Colin et al., 2010). The relatively low $\delta^{18}O_w$ values during the LGM and deglacial period have been linked to a decrease in sea surface salinity and a great influence of freshwater discharge from the Mekong River (Fig. 3f; Colin et al., 2010). During low sea-level of the last glacial period (around −120 m below the present-day level; Lambeck et al., 2014), the paleo-Molengraaff River was exposed on the Sunda shelf (Steinke et al., 2006; Hanebuth et al., 2011) while the Paleo-Mekong River mouth shifted seaward and was only 100 km away from core MD01–2393 (Liu et al., 2005) (Fig. 1c, 3a). In this land-sea configuration, the studied site would have been more sensitive to freshwater river discharge which would also have induced a general decrease in the sea surface salinity.

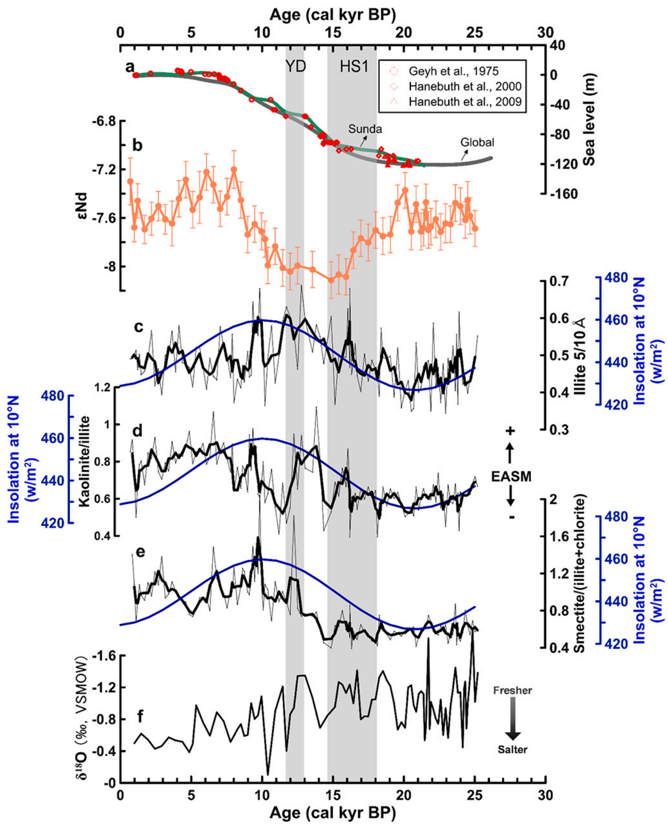

Fig. 3. Sea-level changes and geochemistry and clay mineral records of core MD01–2393 for the last 25 kyrs. (a) Eustasy and sea-level curve for the Sunda Shelf (Hanebuth et al., 2009); (b) foraminiferal εNd (this study); (c) illite chemistry index (Colin et al., 2010); (d) kaolinite/ illite ratio (Colin et al., 2010); (e) smectite/(illite+chlorite) ratio (Colin et al., 2010); (f) $\delta^{18}O_w$ record (Colin et al., 2010). The blue curves shown in figures c, d, e are the Summer insolation curves at 10°N during June–July. (For interpretation of the references to colour in this figure legend, the reader is referred to the web version of this article.)

The emersion of the continental shelves led to large inputs of terrigenous sediment from the Mekong River basin and of reworked shelf sediments to core MD01–2393. This induced higher sedimentation rates during the LGM (mean value of 55.4 cm/kyr) than during the Holocene (mean value of 19 cm/kyr) for core MD01–2393. Such changes in sedimentation rates have also been observed in most cores from the south-western SCS where sedimentation rates during the last glacial period (average sedimentation rate > 70 cm/kyr) are higher than those of the Holocene (average sedimentation rate of ~12 cm/kyr) (Wong et al., 2003).

However, greater lithogenic Nd inputs from rivers which are characterized by unradiogenic Nd isotopic composition during glacial low sea-level stand are not associated with more negative seawater εNd values at the studied site than the Holocene, in which there is less detrital discharge from Mekong River during high sea-level stand (Fig. 3b). On the contrary, foraminiferal εNd of the LGM and the late Holocene are similar. This suggests that variations in the intensity of freshwater and sediment discharges from the Paleo-Mekong River are not the main reason for past changes in foraminiferal εNd off the mouth of the Mekong River, at least during the last 25 cal kyr BP.

5.2.2. *Intensity of sediment weathering*

In Fig. 3, the foraminiferal εNd record has been compared with the mineralogical compositions of sediments delivered from the Mekong River basin to core MD01–2393 over the last 25 kyr (Liu et al., 2005; Colin et al., 2010). The decrease in foraminiferal εNd between 18 and 12 cal kyr BP is associated with an increase in the illite chemistry index (illite 5/10 Å), the kaolinite/illite ratio and the smectite/(illite+chlorite) ratio.

An increase in the kaolinite/illite and smectite/(illite+chlorite) mineralogical ratios indicates a decrease in the relative proportion of primary minerals (such as illite and chlorite) deriving from physical erosion of the eastern Tibetan Plateau, and a relative increase in secondary minerals (such as smectite and kaolinite) deriving from plain soils of the Mekong River basin where intensive chemical weathering takes place (Liu et al., 2004). Such clay mineralogical ratios reflect the history of chemical weathering versus physical erosion on the eastern Tibetan Plateau and in the Mekong River Basin. The illite chemistry index calculated by the ratio of 5 Å and 10 Å illite peak areas in XRD diagrams (Esquevin, 1969) can also be used as an indicator of the intensity of chemical weathering of illite in southern Chinese river sediments (Liu et al., 2007). Higher ratios are found in Al-rich illites (muscovites), which are released following strong hydrolysis; when Mg and Fe substitute Al in the crystal lattice of illite under strong physical erosion, ratios decrease accordingly and thus represent Fe—Mg rich illites (biotites) (Liu et al., 2012; Rainer et al., 1996). Consequently, a higher illite chemistry index is associated with stronger hydrolysis conditions on land, whereas lower illite chemistry index is associated with dominant physical erosion.

The illite chemistry index (Fig. 3c) and the kaolinite/illite ratio (Fig. 3d) of core MD01–2393 increase at around 18 cal kyr BP, suggesting a strengthening of chemical weathering in the Mekong River basin at 18 cal kyr BP (Liu et al., 2004; Sang et al., 2022). Foraminiferal εNd records display a decrease in values at 18 cal kyr BP coeval with the increase in the chemical weathering state of sediments delivered efficiently to the margin by the Paleo-Mekong River. By contrast, higher foraminiferal εNd values are found during the LGM when the Paleo-Mekong River discharge was high but characterized by sediment inputs resulting from strong physical erosion of the highlands of the eastern Tibetan Plateau (high relative proportion of illite and chlorite). During the Holocene, a decrease in chemical weathering intensity, as well as a drop in freshwater discharge to the studied site, corresponds to relatively radiogenic values. We can thus suggest that mineral weathering of pedogenic minerals (e.g., smectite, kaolinite, iron oxides and other pedogenic minerals) in the Mekong River basin might play a major role in the Nd exchange between particulates and seawater. This is supported by the recent finding that a greater state of weathering of sedimentary rock might promote the reactivity of REE exchange between detrital sediments and seawater (Larkin et al., 2021; Huang et al., 2023).

The sea surface hydrology in the SCS and chemical weathering variations on land are both greatly influenced by the East Asian Summer Monsoon (EASM) (Steinke et al., 2006; Huang et al., 2018; Yin et al., 2021; Liu et al., 2007). It has been reported that the stronger chemical weathering and lower $\delta^{18}O_w$ in core MD01–2393 since 18 cal kyr BP are related to increasing EASM rainfall in the Mekong River basin (Colin et al., 2010; Jiwarungrueangkul and Liu, 2021). Long-term variations in weathering intensity and foraminiferal εNd co-vary with the insolation curve received by the earth at 10°N of latitude, which is the main control on past EASM intensity in the studied area.

Overall, the εNd values in the southern core are linked to the state of hydrolysis of minerals from the Mekong River catchment input to the SCS mainly controlled by the EASM rainfall intensity changes and by re-routing of sediments transported from land due to sea-level changes.

5.3. *Variations of εNd values in the northern SCS*

The foraminiferal εNd records in core MD18–3569 display relatively stable and similar εNd values during last the glacial and late Holocene periods, as was also observed in the southern SCS core MD01–2393. However, core MD18–3569 features a continuous increase of εNd from 18 to 12 cal kyr BP, reaching a maximum of −5.8 ± 0.2 at around 12 cal kyr BP (Fig. 4a). This evolution of foraminiferal εNd contrasts with the

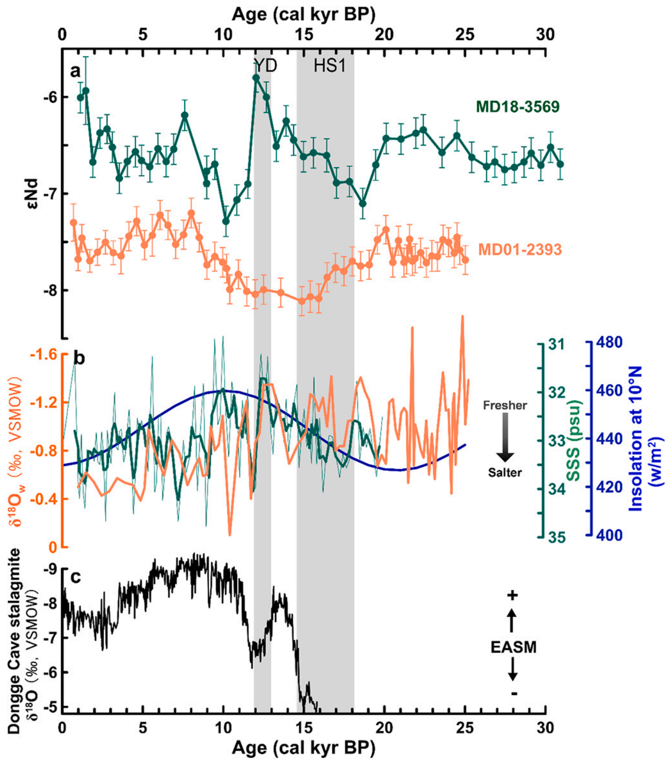

Fig. 4. (a) εNd records of mixed planktonic foraminifera species in core MD18–3569 (green line) and core MD01–2393 (orange line); (b) sea surface salinity (SSS) in core MD18–3569 (green line, Chen et al., 2021) and δ^{18}Ow record obtained on core MD01–2393 (orange line, Colin et al., 2010), summer insolation curve at 10°N of latitude during June–July (blue line); (c) Dongge cave stalagmite δ^{18}O curve (Dykoski et al.,2005). (For interpretation of the references to colour in this figure legend, the reader is referred to the web version of this article.)

foraminiferal εNd record obtained in the southern SCS where the time interval between 18 and 12 cal kyr BP is associated with unradiogenic εNd values.

Two decreases in the εNd values are recognized between 20 and 18 cal kyr BP and between 12 and 10 cal kyr BP, respectively. These decreases have been already observed in cores SO17940–2 and MD05–2904 (Huang et al., 2014; Wu et al., 2017). It has already been proposed that such shifts to more negative εNd values in the northern SCS are not induced by a higher proportion of southern source waters, which are characterized in the southern Ocean by negative values (εNd values of the Circumpolar Deep Water range from −9 to −8; Carter et al., 2012, Amakawa et al., 2013), but are instead associated with a greater influence of terrigenous discharge from Asian rivers (Wu et al., 2017). However, in core MD18–3569, the relatively stable Nd isotope compositions ($-6.7 \pm 0.2 \sim -6.3 \pm 0.2$) during the 30–20 cal kyr BP interval are not compatible with the most negative values (-7.3 ± 0.2) recognized at 10.2 cal kyr BP. This implies that the modification of Nd isotope compositions is less pronounced even though the distance to a river mouth is shorter at low-sea-level stand. Glacial sediments of core MD18–3569 are characterized by content of primary minerals such as illite and chlorite resulting from physical erosion, and which are thus less efficient in modifying the dissolved εNd values, as in the southern core. The sharp drop in εNd values during the 12–10 kyr BP interval may correspond to an increase in sediment discharge from Taiwanese rivers under more intense chemical weathering conditions caused by strong EASM rainfall and a rapid rise of sea-level (Hanebuth et al., 2000; Hsieh et al., 2006).

However, the increase in the input of detrital materials experiencing higher chemical weathering and/or physical erosions fails to explain the continuous increase in εNd values in the northern core during the 18–12 cal kyr interval. Considering that core MD18–3569 is located in the pathway of the intermediate water inflows from the Pacific Ocean, we can reasonably hypothesize that the εNd tendency towards radiogenic values during the deglacial period mainly resulted from a change in water masses from the Pacific Ocean or from hydrological changes within the SCS.

5.4. *Past hydrological implications of the SCS*

Considering different time resolutions of the foraminiferal εNd records and potential problems of age model, core MD18–3569 (1320 m water depth) shares similar temporal variations (from 18 to 12 kyr) of εNd values with cores MD05–2904 (2066 m) and SO17940 (1727 m) located in the northern SCS (Fig. 1b, Fig. 5a, Wu et al., 2017, Huang et al., 2014), which indicates that the three core sites, at different water depths, have recorded a regional signal with some offset between foraminiferal εNd records during the last deglaciation.

A slowdown of circulation within the SCS could be associated with an increase in residence time of deep-water masses in the SCS, which in

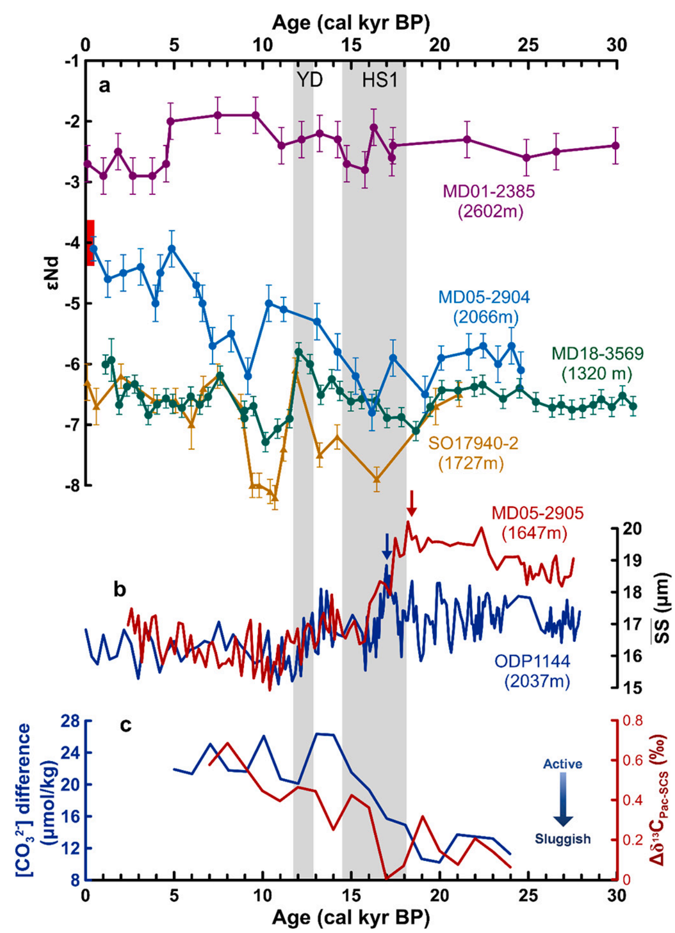

Fig. 5. (a) εNd records of mixed planktonic foraminifera species and leachate in the Philippine Sea (MD01–2395, purple line; Wu et al., 2017) and northern SCS (MD18–3569, green line, this study; MD05–2904, blue line, Wu et al.,2017; SO17940–2, yellow line, Huang et al., 2014), the red square represents the modern range of seawater εNd; (b) Temporal changes in mean sortable silt proxy of sediments in core MD05–2905 and ODP Site 1144 showing changes in stratification conditions in the deep South China Sea (Zhao et al., 2023); (c) gradients of deep water [CO_3^{2-}] (blue line) and δ^{13}C (red line) between the Pacific and the SCS (Wan et al.,2020). (For interpretation of the references to colour in this figure legend, the reader is referred to the web version of this article.)

turn could result in a longer contact time between the deep-water masses (εNd = ~ − 4) and unradiogenic sediments (εNd = ~ − 12, Wei et al., 2012) along the western continental margin of the SCS. In such a scenario, seawater εNd of deep-water of the SCS could also be related to the degree of ventilation of deep-water within the SCS. The increasing trend during the deglacial period in all the northern cores indicates a short contact time between water masses and unradiogenic sediments, and thus a strong ventilation rate in the northern SCS. This strong ventilation and short residence time of deep-water is supported by a recent study which finds increasing gradients of deep water [$CO_3{}^{2-}$] and $\delta^{13}C$ between the Pacific Ocean and the SCS during the deglacial period (from 18 and 13 cal kyr BP) (Fig. 5c, Wan et al., 2020).

The increasing ventilation during this time is interpreted as being associated with a newly formed NPIW in the subarctic Pacific Ocean beginning at about 18 cal kyr BP (Okazaki et al., 2010, Wan and Jian, 2014, Gong et al., 2019). The strengthening of deep currents, deduced on the basis on magnetic properties and sortable silt proxy of sediments in the northern SCS, occurred first at intermediate depth (18.8 cal kyr BP) and then at deep depth (17.2 cal kyr BP) of the northern SCS (Zheng et al., 2016; Zhao et al., 2023). This is also well recorded by our foraminiferal εNd results: the onset towards radiogenic values begins earlier at a shallower depth in core MD18–3569 (1320 m) and later in core MD05–2904 (2066 m). This intrusion was prevented at the end of Younger Dryas by the opening of Bering Strait (Zheng et al., 2016) and it also marked the end of the increasing trend of εNd values in core MD18–3569.

Differences in the radiocarbon dating of coexisting benthic and planktonic foraminifera shells (B—P age) in cores of the southern and northern SCS have been established to record the ventilation age of water masses in the SCS (Fig. 6c; Wan et al., 2014). When combined with the past seawater εNd gradients (ΔεNd) of the two cores in this study (Fig. 6b), we are able to reconstruct the hydrology within the SCS. Indeed, cores MD01–2393 and MD18–3569 are located on similar water mass flowing counter-clockwise in the SCS. Southern core MD01–2393 is strongly influenced by Nd lithogenic inputs from the Mekong Basin and lithogenic inputs to the water mass as it circulates along the western margin of the SCS (Huang et al., 2023). Core MD18–3569 is influenced by the direct influx of PDW from the Philippine Sea, which mixes with more unradiogenic water from the southern SCS via an inter-basin recirculation. During the deglacial period, the young NPIW intrusion is characterized by low B—P age (Wan et al., 2014) and radiogenic εNd values in the northern core, but is not recorded by the southern core (MD01–2393) which is characterized by a high B—P age and unradiogenic εNd values. This results in an increasing ΔεNd, which in turn indicates a weak exchange between the north and south of the SCS during this time interval. The ΔεNd values decrease during the 12–8 cal kyr BP interval as a result of a decrease in the intrusion of the young NPIW intrusion as well as intensive vertical mixing and advection in the southern SCS inducing unradiogenic εNd signature in both cores (Wan et al., 2014).

During the late Holocene period, the εNd records of both cores MD18–3569 and MD01–2393 show similar variations of εNd value. It has been proposed that sea level was rising up to −40 m in late Holocene (Fig. 3a), a critical height to re-open the Karimata Strait to the shallow current throughflow (depth of 40 m) and enhancing deep circulation in the SCS (Zheng et al., 2016). The quick turnover within the SCS may facilitate the co-variations of εNd values on the northern and southern SCS along the western margin. This suggests that the SCS has been well mixed with a high ventilation rate since 8 cal kyr BP, as is evident in modern time.

6. Conclusions

In this study, we have investigated εNd values on the carbonate free-fraction and mixed planktonic foraminifera samples of cores located in the southwestern (core MD01–2393) and northeastern (core MD18–3569) SCS to establish the potential influence of water masses from the Pacific Ocean and lithogenic inputs to intermediate-water of the SCS during the last 25 kyr. We conclude that:

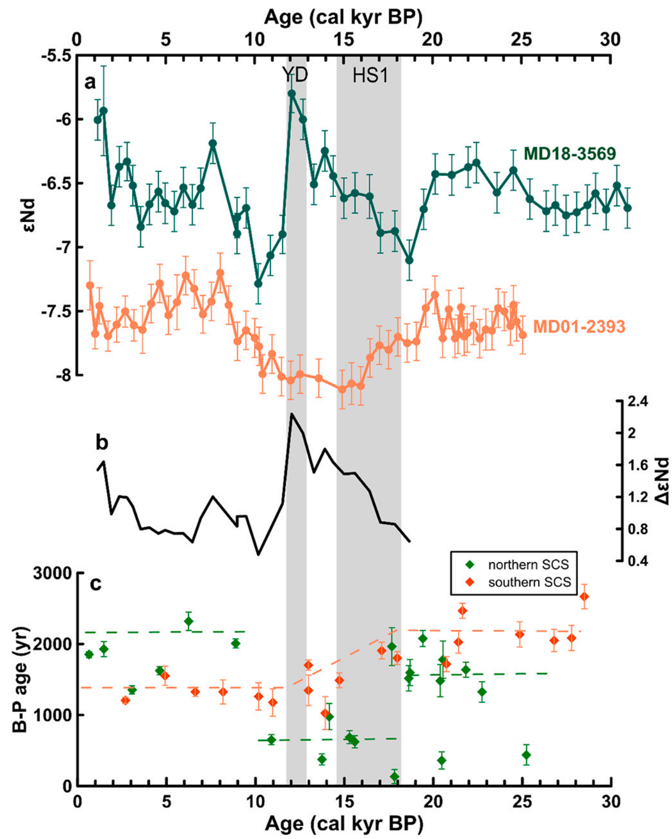

Fig. 6. (a) εNd records of mixed planktonic foraminifera species in cores MD18–3569 (green line) and MD01–2393 (orange line); (b) the ΔεNd values from the difference of two εNd curves (MD18–3569 and MD01–2393); (c) The B—P ages of the northern (MD05–2904 and SO50-37KL, green diamonds) and southern (MD05–2896 and V35–6, orange diamonds) SCS (Wan et al., 2014). (For interpretation of the references to colour in this figure legend, the reader is referred to the web version of this article.)

1. The offset between εNd of the NPIW (−4), which enters the SCS through the Luzon Strait, and foraminiferal εNd obtained from cores MD18–3569 (from −7.3 ± 0.2 to −5.8 ± 0.2) and MD01–2393 (from −8.1 ± 0.2 to −7.2 ± 0.2), results from unradiogenic Nd lithogenic inputs by large Asian rivers. Foraminiferal εNd variations are not associated with any changes in the sedimentary sources which remain the Mekong River basin for core MD01–2393 and SW Taiwan rivers for core MD18–3569. Glacial periods, which are characterized by higher sedimentation rates, are not associated with more unradiogenic Nd signatures. The negative offset of 2 to 3 epsilon units between seawater εNd and foraminiferal samples taken at the top of the two cores are associated with the existence of a benthic flux and an exchange of seawater with detrital particles. The existence of similar εNd variations in other cores from the northern SCS leads to the conclusion that benthic fluxes cannot alone explain all the variability observed in our cores.
2. Variations in the foraminiferal εNd record of core MD01–2393 are coeval with those of the Sea Surface Salinity ($\delta^{18}O_{sw}$) and proxies of the state of chemical weathering of river sediments delivered to the SCS (illite chemical index and kaolinite/illite ratio). During glacial times, the site witnessed large terrigenous fluxes of poorly altered minerals resulting from pronounced physical erosion of the highland of the Mekong River basin; these fluxes are not associated with more

unradiogenic seawater εNd values. On the contrary, foraminiferal εNd displays significantly unradiogenic values during the time interval from 18 to 8 cal kyr BP which are associated with intensification of monsoon rainfall and river input of detrital material characterized by strongly altered minerals (high illite chemical index and kaolinite/illite ratio) deriving from tropical plain soils of the Mekong River basin. This suggests that the modification of dissolved εNd values depends mostly on the inputs of pedogenic minerals (e.g., smectite, kaolinite, iron oxides and other pedogenic minerals) resulting from more intense chemical weathering of the plain soils and thus related to the variations in EASM intensity.

3. Core MD18–3569, located in the northern SCS, displays similar variations to core MD01–2393 with the exception of a decoupled evolution of εNd during the period between 18 and 12 cal kyr BP. During this period, an increasing long term change (from -7.1 ± 0.2 to -5.8 ± 0.2) is identified in core MD18–3569: this change is interpreted as being linked to the intensification of the intrusion of the newly formed glacial NPIW into the SCS. The differences in εNd values between both cores, combined with $\Delta^{14}C$, imply that circulation was relatively sluggish, with reduced water exchange between the North and South SCS during this time interval.

CRediT authorship contribution statement

Yi Huang: Writing – review & editing, Writing – original draft, Visualization, Validation, Methodology, Investigation, Formal analysis, Data curation, Conceptualization. **Christophe Colin:** Writing – review & editing, Writing – original draft, Supervision, Resources, Project administration, Formal analysis, Data curation, Conceptualization. **Zhifei Liu:** Writing – review & editing, Resources. **Bertaz Joffrey:** Writing – review & editing, Investigation. **Arnaud Dapoigny:** Writing – review & editing, Methodology, Formal analysis. **Eric Douville:** Writing – review & editing, Resources. **Zhaojie Yu:** Writing – review & editing. **Andrew Tien-Shun Lin:** Writing – review & editing, Resources.

Declaration of competing interest

The authors declare that they have no known competing financial interests or personal relationships that could have appeared to influence the work reported in this paper.

Data availability

All the data is available on the text and SI.

Acknowledgements

We thank the IFREMER (Institut Polaire Emile Victor), the crews and scientific teams of the HYDROSED research cruise for their excellent work during the cores sampling. Y. Huang acknowledges the CSC for supporting her study in France. We gratefully acknowledge the assistance provided by Louise Bordier during Nd isotope analyses. We especially thank Prof Albert Galy and one anonymous reviewer for their constructive reviews, which significantly helped to improve this manuscript.

Appendix A. Supplementary data

Supplementary data to this article can be found online at https://doi.org/10.1016/j.chemgeo.2024.121954.

References

Abbott, A.N., Haley, B.A., McManus, J., 2016. The impact of sedimentary coatings on the diagenetic Nd flux. Earth Planet. Sci. Lett. 449, 217–227.
Abbott, A.N., Löhr, S., Trethewy, M., 2019. Are clay minerals the primary control on the Oceanic rare Earth element budget? Front. Mar. Sci. 6, 504.
Amakawa, H., Alibo, D.S., Nozaki, Y., 2000. Nd isotopic composition and REE pattern in the surface waters of the eastern Indian Ocean and its adjacent seas. Geochim. Cosmochim. Acta 64, 1715–1727.
Amakawa, H., Nozaki, Y., Alibo, D.S., Zhang, J., Fukugawa, K., Nagai, H., 2004. Neodymium isotopic variations in Northwest Pacific waters. Geochim. Cosmochim. Acta 68, 715–727.
Amakawa, H., Sasaki, K., Ebihara, M., 2009. Nd isotopic composition in the central North Pacific. Geochim. Cosmochim. Acta 73, 4705–4719.
Amakawa, H., Tazoe, H., Obata, H., Gamo, T., Sano, Y., Shen, C.-C., 2013. Neodymium isotopic composition and concentration in the Southwest Pacific Ocean. Geochem. J. 47, 409–422.
Bang, S., Huh, Y., Khim, B.-K., Takata, H., Ikehara, M., Hyeong, K., Seo, I., Cho, H., 2021. Deep-water circulation over the last two glacial cycles reconstructed from authigenic neodymium isotopes in the equatorial Indian Ocean (Core HI1808-GPC04). Ocean Sci. J. 57, 324–333.
Bayon, G., Giresse, P., Chen, H., Rouget, M.-L., Gueguen, B., Moizinho, G.R., Barrat, J.-A., Beaufort, D., 2023. The behavior of rare earth elements during green clay authigenesis on the congo continental shelf. Minerals 13, 1081.
Blanckenburg, F.V., Nagler, T.F., 2001. Weathering versus circulation-controlled changes in radiogenic isotope tracer composition of the Labrador Sea and North Atlantic Deep Water. Paleoceanography 16, 424–434.
Blaser, P., Lippold, J., Gutjahr, M., Frank, N., Link, J.M., Frank, M., 2016. Extracting foraminiferal seawater Nd isotope signatures from bulk deep sea sediment by chemical leaching. Chem. Geol. 439, 189–204.
Boulay, S., Colin, C., Trentesaux, A., Frank, N., Liu, Z., 2005. Sediment sources and East Asian monsoon intensity over the last 450 ky. Mineral. Geochem. Investig. South China Sea Sediment. Palaeogeogr. Palaeoclimatol. Palaeoecol. 228, 260–277.
Broecker, W., Clark, E., Barker, S., 2008. Near constancy of the Pacific Ocean surface to mid-depth radiocarbon-age difference over the last 20 kyr. Earth Planet. Sci. Lett. 274, 322–326.
Burton, K.W., Vance, D., 2000. Glacial-interglacial variations in the neodymium isotope composition of seawater in the Bay of Bengal recorded by planktonic foraminifera. Earth Planet. Sci. Lett. 425–441.
Carter, P., Vance, D., Hillenbrand, C.D., Smith, J.A., Shoosmith, D.R., 2012. The neodymium isotopic composition of waters masses in the eastern Pacific sector of the Southern Ocean. Geochim. Cosmochim. Acta 79, 41–59.
Chang, Y.-T., Hsu, W.-L., Tai, J.-H., Tang, T.Y., Chang, M.-H., Chao, S.-Y., 2010. Cold Deep Water in the South China Sea. J. Oceanogr. 66, 183–190.
Chen, Q., Liu, Z., Kissel, C., 2017. Clay mineralogical and geochemical proxies of the East Asian summer monsoon evolution in the South China Sea during late Quaternary. Sci. Rep. 7, 42083.
Chen, Y., Wang, Y., Dang, H., Jian, Z., 2021. Hydroclimatic changes in the northeastern South China Sea since the last glacial maximum. Quatern. Sci. 41, 1031–1043.
Colin, C., Siani, G., Sicre, M.A., Liu, Z., 2010. Impact of the East Asian monsoon rainfall changes on the erosion of the Mekong River basin over the past 25,000yr. Mar. Geol. 271, 84–92.
Copard, K., Colin, C., Douville, E., Freiwald, A., Gudmundsson, G., De Mol, B., Frank, N., 2010. Nd isotopes in deep-sea corals in the North-eastern Atlantic. Quat. Sci. Rev. 29, 2499–2508.
Du, J., Haley, B.A., Mix, A.C., 2016. Neodymium isotopes in authigenic phases, bottom waters and detrital sediments in the Gulf of Alaska and their implications for paleo-circulation reconstruction. Geochim. Cosmochim. Acta 193, 14–35.
Dubois-Dauphin, Q., Colin, C., Bonneau, L., Montagna, P., Wu, Q., Van Rooij, D., Reverdin, G., Douville, E., Thil, F., Waldner, A., Frank, N., 2017. Fingerprinting Northeast Atlantic water masses using neodymium isotopes. Geochim. Cosmochim. Acta 210, 267–288.
Duy Vinh, V., Ouillon, S., Van Thao, N., Ngoc Tien, N., 2016. Numerical simulations of suspended sediment dynamics due to seasonal forcing in the Mekong Coastal Area. Water 8, 255.
Esquevin, J., 1969. Influence de la composition chimique des illites surcristallinite. Bull. Cent. Rech. Rau-SNP A 3, 147–153.
Frank, M., 2002. Radiogenic Isotopes: Tracers of Past Ocean Circulation and Erosional Input. Rev. Geophys. 40, 1-1-1-38.
Fuhr, M., Laukert, G., Yu, Y., Nürnberg, D., Frank, M., 2021. Tracing water mass mixing from the Equatorial to the North Pacific Ocean with dissolved neodymium isotopes and concentrations. Front. Mar. Sci. 7, 603761.
Gong, X., Lembke-Jene, L., Lohmann, G., Knorr, G., Tiedemann, R., Zou, J.J., Shi, X.F., 2019. Enhanced North Pacific deep-ocean stratification by stronger intermediate water formation during Heinrich Stadial 1. Nat. Commun. 10, 656.
Gourlan, A.T., Meynadier, L., Allègre, C.J., 2008. Tectonically driven changes in the Indian Ocean circulation over the last 25 Ma: Neodymium isotope evidence. Earth Planet. Sci. Lett. 267, 353–364.
Gourlan, A.T., Meynadier, L., Allègre, C.J., Tapponnier, P., Birck, J.-L., Joron, J.-L., 2010. Northern Hemisphere climate control of the Bengali rivers discharge during the past 4 Ma. Quat. Sci. Rev. 29, 2484–2498.
Grasse, P., Stichel, T., Stumpf, R., Stramma, L., Frank, M., 2012. The distribution of neodymium isotopes and concentrations in the Eastern Equatorial Pacific: Water mass advection versus particle exchange. Earth Planet. Sci. Lett. 353-354, 198–207.
Hanebuth, T.J.J., Stattegger, K., Bojanowski, A., 2009. Termination of the Last Glacial Maximum sea-level lowstand: The Sunda-Shelf data revisited. Glob. Planet Change 66, 76–84.
Hanebuth, T., Stattegger, K., Grootes, P.M., 2000. Rapid Flooding of the Sunda Shelf: A Late-Glacial Sea-Level Record. Science 288, 1033–1035.
Hanebuth, T.J.J., Voris, H.K., Yokoyama, Y., Saito, Y., Okuno, J., i., 2011. Formation and fate of sedimentary depocentres on Southeast Asia's Sunda Shelf over the past sea-level cycle and biogeographic implications. Earth Sci. Rev. 104, 92–110.

Hindshaw, R.S., Aciego, S.M., Piotrowski, A.M., Tipper, E.T., 2018. Decoupling of dissolved and bedrock neodymium isotopes during sedimentary cycling. Geochem. Perspect. Lett. 8, 43–46.
Howe, J.N.W., Piotrowski, A.M., Rennie, V.C.F., 2016. Abyssal origin for the early Holocene pulse of unradiogenic neodymium isotopes in Atlantic seawater. Geology 44, 831–834.
Hsieh, M.-L., Lai, T.-H., Wu, L.-C., Lu, W.-C., Liu, H.-T., Liew, P.-M., 2006. Eustatic Sea-level change of 11–5 ka in Western Taiwan, constrained by radiocarbon dates of core sediments. Terr. Atmos. Ocean. Sci. 17, 353–370.
Hu, D., Böning, P., Köhler, C.M., Hillier, S., Pressling, N., Wan, S., Brumsack, H.J., Clift, P.D., 2012. Deep sea records of the continental weathering and erosion response to East Asian monsoon intensification since 14ka in the South China Sea. Chem. Geol. 326-327, 1–18.
Hu, R., Piotrowski, A.M., Bostock, H.C., Crowhurst, S., Rennie, V., 2016. Variability of neodymium isotopes associated with planktonic foraminifera in the Pacific Ocean during the Holocene and last Glacial Maximum. Earth Planet. Sci. Lett. 447, 130–138.
Huang, E., Chen, Y., Schefuß, E., Steinke, S., Liu, J., Tian, J., Martínez-Méndez, G., Mohtadi, M., 2018. Precession and glacial-cycle controls of monsoon precipitation isotope changes over East Asia during the Pleistocene. Earth Planet. Sci. Lett. 494, 1–11.
Huang, K.-F., You, C.-F., Chung, C.-H., Lin, Y.-H., Liu, Z., 2014. Tracing the Nd isotope evolution of North Pacific Intermediate and Deep Waters through the last deglaciation from South China Sea sediments. J. Asian Earth Sci. 79, 564–573.
Huang, Y., Colin, C., Liu, Z., Douville, E., Dapoigny, A., Haurine, F., Wu, Q., Lin, T., 2023. Impacts of nepheloid layers and mineralogical compositions of oceanic margin sediments on REE concentrations and Nd isotopic compositions of seawater. Geochim. Cosmochim. Acta 359, 57–70.
Jacobsen, S.B., Wasserburg, G.J., 1980. Sm-Nd isotopic evolution of chondrites. Earth Planet. Sci. Lett. 50, 139–155.
Jang, K., Bayon, G., Han, Y., Joo, Y.J., Kim, J.-H., Ryu, J.-S., Woo, J., Forwick, M., Szczuciński, W., Kim, J.-H., Nam, S.-I., 2020. Neodymium isotope constraints on chemical weathering and past glacial activity in Svalbard. Earth Planet. Sci. Lett. 542, 116319.
Jeandel, C., Arsouze, T., Lacan, F., Téchiné, P., Dutay, J.C., 2007. Isotopic Nd compositions and concentrations of the lithogenic inputs into the ocean: A compilation, with an emphasis on the margins. Chem. Geol. 239, 156–164.
Jeandel, C., Delattre, H., Grenier, M., Pradoux, C., Lacan, F., 2013. Rare earth element concentrations and Nd isotopes in the Southeast Pacific Ocean. Geochem. Geophys. Geosyst. 14, 328–341.
Jian, Z., Wang, L., Kienast, M., Sarnthein, M., Kuhnt, W., Lin, H., Wang, P., 1999. Benthic foraminiferal paleoceanography of the South China Sea over the last 40,000 years. Mar. Geol. 156, 159–186.
Jin, H., Jian, Z., Wan, S., 2018. Recent deep water ventilation in the South China Sea and its paleoceanographic implications. Deep-Sea Res. I Oceanogr. Res. Pap. 139, 88–94.
Jiwarungrueangkul, T., Liu, Z., 2021. East Asian monsoon and sea-level controls on clay mineral variations in the southern South China Sea since the last Glacial Maximum. Quat. Int. 592, 1–11.
Kawabe, M., Fujio, S., 2010. Pacific Ocean circulation based on observation. J. Oceanogr. 66, 389–403.
Kraft, S., Frank, M., Hathorne, E.C., Weldeab, S., 2013. Assessment of seawater Nd isotope signatures extracted from foraminiferal shells and authigenic phases of Gulf of Guinea sediments. Geochim. Cosmochim. Acta 121, 414–435.
Lambeck, K., Rouby, H., Purcell, A., Sun, Y., Sambridge, M., 2014. Sea level and global ice volumes from the last Glacial Maximum to the Holocene. Proc. Natl. Acad. Sci. USA 111, 15296–15303.
Larkin, C.S., Piotrowski, A.M., Hindshaw, R.S., Bayon, G., Hilton, R.G., Baronas, J.J., Dellinger, M., Wang, R., Tipper, E.T., 2021. Constraints on the source of reactive phases in sediment from a major Arctic river using neodymium isotopes. Earth Planet. Sci. Lett. 565, 116933.
Levitus, S., Burgett, R., Boyer, T., 1994. World Ocean Atlas.
Li, B., Wang, J., Huang, B., Li, Q., Jian, Z., Zhao, Q., Su, X., Wang, P., 2004. South China Sea surface water evolution over the last 12 Myr: A south-north comparison from Ocean Drilling Program Sites 1143 and 1146. Paleoceanography 19.
Li, L., Qu, T., 2006. Thermohaline circulation in the deep South China Sea basin inferred from oxygen distributions. J. Geophys. Res. 111, C5.
Liu, Z., Gan, J., 2017. Three-dimensional pathways of water masses in the South China Sea: A modeling study. J. Geophys. Res. Oceans 122, 6039–6054.
Liu, Z., Stattegger, K., 2014. South China Sea fluvial sediments: an introduction. J. Asian Earth Sci. 79, 507–508.
Liu, Z., Colin, C., Trentesaux, A., Blamart, D., Bassinot, F., Siani, G., Sicre, M.-A., 2004. Erosional history of the eastern Tibetan Plateau since 190 kyr ago: clay mineralogical and geochemical investigations from the southwestern South China Sea. Mar. Geol. 209, 1–18.
Liu, Z., Colin, C., Trentesaux, A., Siani, G., Frank, N., Blamart, D., Farid, S., 2005. Late Quaternary climatic control on erosion and weathering in the eastern Tibetan Plateau and the Mekong Basin. Quat. Res. 63, 316–328.
Liu, Z., Colin, C., Huang, W., Le, K.P., Tong, S., Chen, Z., Trentesaux, A., 2007. Climatic and tectonic controls on weathering in South China and Indochina Peninsula: Clay mineralogical and geochemical investigations from the Pearl, Red, and Mekong drainage basins. Geochem. Geophys. Geosyst. 8, Q05005.
Liu, Z., Colin, C., Li, X., Zhao, Y., Tuo, S., Chen, Z., Siringan, F.P., Liu, J.T., Huang, C.-Y., You, C.-F., Huang, K.-F., 2010. Clay mineral distribution in surface sediments of the northeastern South China Sea and surrounding fluvial drainage basins: source and transport. Mar. Geol. 277, 48–60.
Liu, Z., Wang, H., Hantoro, W.S., Sathiamurthy, E., Colin, C., Zhao, Y., Li, J., 2012. Climatic and tectonic controls on chemical weathering in tropical Southeast Asia (Malay Peninsula, Borneo, and Sumatra). Chem. Geol. 291, 1–12.
Liu, Z., Zhao, Y., Colin, C., Stattegger, K., Wiesner, M.G., Huh, C.-A., Zhang, Y., Li, X., Sompongchaiyakul, P., You, C.-F., Huang, C.-Y., Liu, J.T., Siringan, F.P., Le, K.P., Sathiamurthy, E., Hantoro, W.S., Liu, J., Tuo, S., Zhao, S., Zhou, S., He, Z., Wang, Y., Bunsomboonsakul, S., Li, Y., 2016. Source-to-sink transport processes of fluvial sediments in the South China Sea. Earth Sci. Rev. 153, 238–273.
Matsumoto, K., Oba, T., Lynch-Stieglitz, J., Yamamoto, H., 2002. Interior hydrography and circulation of the glacial Pacific Ocean. Quat. Sci. Rev. 21, 1693–1704.
Milliman, J.D., Farnsworth, K.L., 2011. River Discharge to the Coastal Ocean: A Global Synthesis. Cambridge University Press, Cambridge.
Montagna, P., Colin, C., Frank, M., Störling, T., Tanhua, T., Rijkenberg, M.J.A., Taviani, M., Schroeder, K., Chiggiato, J., Gao, G., Dapoigny, A., Goldstein, S.L., 2022. Dissolved neodymium isotopes in the Mediterranean Sea. Geochim. Cosmochim. Acta 322, 143–169.
Okazaki, Y., Timmermann, A., Menviel, L., Harada, N., Abe-Ouchi, A., Chikamoto, M.O., Mouchet, A., Asahi, H., 2010. Deepwater Formation in the North Pacific during the last Glacial termination. Science 329, 200–203.
Okazaki, Y., Sagawa, T., Asahi, H., Horikawa, K., Onodera, J., 2012. Ventilation changes in the western North Pacific since the last glacial period. Clim. Past 8, 17–24.
Osborne, A.H., Haley, B.A., Hathorne, E.C., Flögel, S., Frank, M., 2014. Neodymium isotopes and concentrations in Caribbean seawater: Tracing water mass mixing and continental input in a semi-enclosed ocean basin. Earth Planet. Sci. Lett. 406, 174–186.
Piotrowski, A.M., Goldstein, S.L., Hemming, S.R., Fairbanks, R.G., 2005. Temporal relationships of carbon cycling and ocean circulation at glacial boundaries. Science 307, 1933–1938.
Piotrowski, A.M., Galy, A., Nicholl, J.A.L., Roberts, N., Wilson, D.J., Clegg, J.A., Yu, J., 2012. Reconstructing deglacial North and South Atlantic deep water sourcing using foraminiferal Nd isotopes. Earth Planet. Sci. Lett. 357-358, 289–297.
Pomie's, C., Davies, G.R., Conan, S.M.-H., 2002. Neodymium in modern foraminifera from the Indian Ocean: implications for the use of foraminiferal Nd isotope compositions in paleooceanography. Earth Planet. Sci. Lett. 203, 1031–1045.
Qu, T., Du, Y., Sasaki, H., 2006. South China Sea throughflow: a heat and freshwater conveyor. Geophys. Res. Lett. 33, L23617.
Rainer, P., Gerhard, K., Franz, G., 1996. Clay mineral distribution in surface sediments of the South Atlantic: sources, transport and relation to oceanography. Mar. Geol. 130, 203–229.
Roberts, N.L., Piotrowski, A.M., McManus, J.F., Keigwin, L.D., 2010. Synchronous deglacial overturning and water mass source changes. Science 327, 75–78.
Roberts, N.L., Piotrowski, A.M., Elderfield, H., Eglinton, T.I., Lomas, M.W., 2012. Rare earth element association with foraminifera. Geochim. Cosmochim. Acta 94, 57–71.
Rousseau, T.C., Sonke, J.E., Chmeleff, J., van Beek, P., Souhaut, M., Boaventura, G., Seyler, P., Jeandel, C., 2015. Rapid neodymium release to marine waters from lithogenic sediments in the Amazon estuary. Nat. Commun. 6, 7592.
Sang, P.N., Liu, Z., Colin, C., 2022. Chemical Weathering of the Mekong River Basin with Implication for East Asian Monsoon Evolution during the late Quaternary: marine sediment records in the Southern South China Sea. Front. Earth Sci. 10, 885547.
Singh, S.P., Singh, S.K., Goswami, V., Bhushan, R., Rai, V.K., 2012. Spatial distribution of dissolved neodymium and εNd in the Bay of Bengal: Role of particulate matter and mixing of water masses. Geochim. Cosmochim. Acta 94, 38–56.
Steinke, S., Chiu, H.-Y., Yu, P.-S., Shen, C.-C., Erlenkeuser, H., Löwemark, L., Chen, M.-T., 2006. On the influence of sea level and monsoon climate on the southern South China Sea freshwater budget over the last 22,000 years. Quat. Sci. Rev. 25, 1475–1488.
Stichel, T., Hartman, A.E., Duggan, B., Goldstein, S.L., Scher, H., Pahnke, K., 2015. Separating biogeochemical cycling of neodymium from water mass mixing in the Eastern North Atlantic. Earth Planet. Sci. Lett. 412, 245–260.
Tachikawa, K., Piotrowski, A.M., Bayon, G., 2014. Neodymium associated with foraminiferal carbonate as a recorder of seawater isotopic signatures. Quat. Sci. Rev. 88, 1–13.
Tanaka, T., Togashi, S., Kagami, H., Yoneda, S., Yanagi, T., Asahara, Y., Hamamoto, A., Kamioka, H., Yuhara, M., Tanimizu, M., Orihashi, H.A., Shimizu, H., Kunimaru, T., Takahashi, K., Nakano, T., Shinjo, H.F.R., Dragusanu, C., 2000. JNdi-1: a neodymium isotopic reference in consistency with LaJolla neodymium. Chem. Geol. 168, 279–281.
Tian, J., Zhao, W., Yang, Q., 2009. Enhanced diapycnal mixing in the South China Sea. J. Phys. Oceanogr. 39, 3191–3203.
Wan, S., Jian, Z., 2014. Deep water exchanges between the South China Sea and the Pacific since the last glacial period. Paleoceanography 29, 1162–1178.
Wan, S., Jian, Z., Dang, H., 2018. Deep Hydrography of the South China Sea and Deep Water Circulation in the Pacific since the last Glacial Maximum. Geochem. Geophys. Geosyst. 19, 1447–1463.
Wan, S., Jian, Z., Gong, X., Dang, H., Wu, J., Qiao, P., 2020. Deep water [CO_3^{2-}] and circulation in the South China Sea over the last glacial cycle. Quat. Sci. Rev. 243, 106499.
Wang, A., Du, Y., Peng, S., Liu, K., Huang, R.X., 2018. Deep water characteristics and circulation in the South China Sea. Deep-Sea Res. I Oceanogr. Res. Pap. 134, 55–63.
Wang, G., Xie, S.-P., Qu, T., Huang, R.X., 2011. Deep South China Sea circulation. Geophys. Res. Lett. 38, L05601.
Wang, P., Clemens, S., Beaufort, L., Braconnot, P., Ganssen, G., Jian, Z., Kershaw, P., Sarnthein, M., 2005. Evolution and variability of the Asian monsoon system: state of the art and outstanding issues. Quat. Sci. Rev. 24, 595–629.
Wang, R., Clegg, J.A., Scott, P.M., Larkin, C.S., Deng, F., Thomas, A.L., Zheng, X.-Y., Piotrowski, A.M., 2021. Reversible scavenging and advection – Resolving the

neodymium paradox in the South Atlantic. Geochim. Cosmochim. Acta 314, 121–139.

Wang, R., Williams, T.J., Hillenbrand, C.-D., Ehrmann, W., Larkin, C.S., Hutchings, A.M., Piotrowski, A.M., 2022. Boundary processes and neodymium cycling along the Pacific margin of West Antarctica. Geochim. Cosmochim. Acta 327, 1–20.

Wang, R.-M., You, C.-F., Chu, H.-Y., Hung, J.-J., 2009. Seasonal variability of dissolved major and trace elements in the Gaoping (Kaoping) river Estuary, Southwestern Taiwan. J. Mar. Syst. 76, 444–456.

Wang, Y.J., Cheng, H., Edwards, R.L., An, Z.S., Wu, J.Y., Shen, C.-C., Dorale, J.A., 2001. A High-Resolution Absolute-Dated late Pleistocene Monsoon Record from Hulu Cave, China. Science 294, 2345–2348.

Wei, G., Liu, Y., Ma, J., Xie, L., Chen, J., Deng, W., Tang, S., 2012. Nd, Sr isotopes and elemental geochemistry of surface sediments from the South China Sea: Implications for Provenance Tracing. Mar. Geol. 319-322, 21–34.

Wong, H.K., Lüdmann, T., Haft, C., Paulsen, A.-M., Hübscher, C., Geng, J., 2003. Quaternary Sedimentation in the Molengraaff Paleo-Delta, Northern Sunda Shelf (Southern South China Sea). In: Tropical Deltas of Southeast Asia—Sedimentology, Stratigraphy, and Petroleum Geology. SEPM Society for Sedimentary Geology.

Wu, Q., Colin, C., Liu, Z., Douville, E., Dubois-Dauphin, Q., Frank, N., 2015a. New insights into hydrological exchange between the South China Sea and the Western Pacific Ocean based on the Nd isotopic composition of seawater. Deep-Sea Res. II Top. Stud. Oceanogr. 122, 25–40.

Wu, Q., Colin, C., Liu, Z., Thil, F., Dubois-Dauphin, Q., Frank, N., Tachikawa, K., Bordier, L., Douville, E., 2015b. Neodymium isotopic composition in foraminifera and authigenic phases of the South China Sea sediments: Implications for the hydrology of the North Pacific Ocean over the past 25 kyr. Geochem. Geophys. Geosyst. 16, 3883–3904.

Wu, Q., Colin, C., Liu, Z., Bassinot, F., Dubois-Dauphin, Q., Douville, E., Thil, F., Siani, G., 2017. Foraminiferal εNd in the deep north-western subtropical Pacific Ocean: Tracing changes in weathering input over the last 30,000 years. Chem. Geol. 470, 55–66.

Wu, Q., Liu, Z., Colin, C., Douville, E., Zhao, Y., Wu, J., Dapoigny, A., Bordier, L., Ma, P., Huang, Y., 2022. Dissolved rare earth element and neodymium isotope distributions in the South China Sea: Water mass source versus particle dissolution. Front. Mar. Sci. 9, 1003749.

Wyrtki, K., 1961. Physical Oceanography of the Southeast Asian Waters. The university of California.

Xie, L., Tian, J., Zhang, S., Zhang, Y., Yang, Q., 2011. An anticyclonic eddy in the intermediate layer of the Luzon Strait in Autumn 2005. J. Oceanogr. 67, 37–46.

Yin, J., Yang, X., Zhou, Q., Li, G., Gao, H., Liu, J., 2021. Sea surface temperature and salinity variations from the end of last Glacial Maximum (LGM) to the Holocene in the northern South China Sea. Palaeogeogr. Palaeoclimatol. Palaeoecol. 562, 110102.

Yu, Z., Colin, C., Douville, E., Meynadier, L., Duchamp-Alphonse, S., Sepulcre, S., Wan, S., Song, L., Wu, Q., Xu, Z., Bassinot, F., 2017a. Yttrium and rare earth element partitioning in seawaters from the Bay of Bengal. Geochem. Geophys. Geosyst. 18, 1388–1403.

Yu, Z., Colin, C., Meynadier, L., Douville, E., Dapoigny, A., Reverdin, G., Wu, Q., Wan, S., Song, L., Xu, Z., Bassinot, F., 2017b. Seasonal variations in dissolved neodymium isotope composition in the Bay of Bengal. Earth Planet. Sci. Lett. 479, 310–321.

Yu, Z., Colin, C., Ma, R., Meynadier, L., Wan, S., Wu, Q., et al., 2018. Antarctic Intermediate Water penetration into the northern Indian Ocean during the last deglaciation. Earth Planet. Sci. Lett. 500, 67–75.

Yu, Z., Colin, C., Wilson, D.J., Bayon, G., Song, Z., Sepulcre, S., Dapoigny, A., Li, Y., Wan, S., 2022. Millennial Variability in Intermediate Ocean Circulation and Indian Monsoonal Weathering Inputs during the last Deglaciation and Holocene. Geophys. Res. Lett. 49 e2022GL100003.

Zhang, Y., Liu, Z., Zhao, Y., Colin, C., Zhang, X., Wang, M., Zhao, S., Kneller, B., 2018. Long-term in situ observations on typhoon-triggered turbidity currents in the deep sea. Geology 46, 675–678.

Zhao, S., Liu, Z., Colin, C., Zhao, Y., Wang, X., Jian, Z., 2018. Responses of the East Asian Summer Monsoon in the Low-Latitude South China Sea to High-Latitude pe-Scale Climatic changes during the last Glaciation: evidence from a High-Resolution Clay Mineralogical Record. Paleoceanogr. Paleoclimatol. 33, 745–765.

Zhao, Y., Liu, Z., Zhang, Y., Li, J., Wang, M., Wang, W., Xu, J., 2015. In situ observation of contour currents in the northern South China Sea: applications for Deepwater sediment transport. Earth Planet. Sci. Lett. 430, 477–485.

Zhao, Y., Wang, Y., Liu, Z., Li, X., Yang, W., 2023. Deep-water circulation intensity and stratification in the South China Sea since the last glaciation. Mar. Geol. 457, 107004.

Zheng, X., Kao, S., Chen, Z., Menviel, L., Chen, H., Du, Y., Wan, S., Yan, H., Liu, Z., Zheng, L., Wang, S., Li, D., Zhang, X., 2016. Deepwater circulation variation in the South China Sea since the last Glacial Maximum. Geophys. Res. Lett. 43, 8590–8599.

Zhu, Y., Sun, J., Wang, Y., Li, S., Xu, T., Wei, Z., Qu, T., 2019. Overview of the multi-layer circulation in the South China Sea. Prog. Oceanogr. 175, 171–182.